


Altered NMDA receptor-evoked intracellular Ca^{2+} dynamics in magnocellular neurosecretory neurons of hypertensive rats

Meng Zhang and Javier E. Stern 

Department of Physiology, Medical College of Georgia, Augusta University, 1120 15th Street, Augusta, GA 30912, USA

Edited by: Harold Schultz & Julie Chan

Key points

- NMDA receptor (NMDAR)-mediated Ca^{2+} signalling plays a critical role in modulating hypothalamic neurosecretory function. However, whether an altered NMDAR-evoked changes in Ca^{2+} (NMDAR- ΔCa^{2+}) signalling in magnocellular neurosecretory cells (MNCs) may contribute to neurohumoral activation during disease states is unknown.
- We show that activation of NMDARs evoked similar inward currents in MNCs of sham and renovascular hypertensive (RVH) rats. Despite this, a prolonged and larger NMDAR- ΔCa^{2+} response was observed in the latter.
- The exacerbated NMDAR- ΔCa^{2+} responses in MNCs of RVH rats affected both somatic and dendritic compartments.
- Inhibition of the endoplasmic reticulum sarcoendoplasmic reticulum calcium transport ATPase (SERCA) pump prolonged NMDAR- ΔCa^{2+} responses in sham rats, but not in RVH rats.
- Our study supports an altered spatiotemporal dynamic of NMDAR- ΔCa^{2+} signalling in MNCs from RVH rats, partly due to blunted endoplasmic reticulum Ca^{2+} buffering capacity.

Abstract A growing body of evidence supports an elevated NMDA receptor (NMDAR)-mediated glutamate excitatory function in the supraoptic nucleus and paraventricular nucleus of hypertensive rats that contributes to neurohumoral activation in this disease. However, the precise mechanisms underlying altered NMDAR signalling in hypertension remain to be elucidated. In this study, we performed simultaneous electrophysiology and fast confocal Ca^{2+} imaging to determine whether altered NMDAR-mediated changes in intracellular Ca^{2+} levels (NMDAR- ΔCa^{2+}) occurred in hypothalamic magnocellular neurosecretory cells (MNCs) in renovascular hypertensive (RVH) rats. We found that despite evoking a similar excitatory inward current, activation of NMDARs resulted in a larger and prolonged ΔCa^{2+} in MNCs from RVH rats. Changes in NMDAR- ΔCa^{2+} dynamics were observed both in somatic and dendritic compartments. Inhibition of the sarcoendoplasmic reticulum calcium transport ATPase (SERCA) pump activity with thapsigargin prolonged NMDAR- ΔCa^{2+} responses in MNCs of sham rats, but this effect was occluded in RVH rats, thus equalizing the magnitude and time course of the NMDA- ΔCa^{2+} responses between the two experimental groups. Taken together, our results support (1) an exacerbated NMDAR- ΔCa^{2+} response in somatodendritic compartments of MNCs of RVH rats, and (2) that a blunted ER Ca^{2+} buffering capacity contributes to the altered NMDAR- ΔCa^{2+} dynamics in this condition. Thus, altered spatiotemporal dynamics of the NMDAR- ΔCa^{2+} response stands as an underlying mechanism contributing to neurohumoral activation in neurogenic hypertension.

(Received 24 August 2017; accepted after revision 3 October 2017; first published online 15 October 2017)

Corresponding author J. E. Stern: Department of Physiology, Augusta University, 1120 15th St., Augusta, GA 30912, USA. Email: js Stern@augusta.edu

Abbreviations eNMDAR, extrasynaptic NMDAR; ER, endoplasmic reticulum; MNC, magnocellular neurosecretory cell; NMDAR, NMDA receptor; OT, oxytocin; PVN, paraventricular nucleus; RVH rat, renovascular hypertensive rat; SERCA, sarco/endoplasmic reticulum Ca^{2+} -ATPase; SON, supraoptic nucleus; TG, thapsigargin; VP, vasopressin.

Introduction

Vasopressin and oxytocin magnocellular neurosecretory cells (MNCs) of the hypothalamic supraoptic (SON) and paraventricular (PVN) nuclei play critical roles in fluid balance, and cardiovascular and reproductive homeostasis (Silverman & Zimmerman, 1983). Moreover, exacerbated activity of MNCs contributes to neuro-humoral activation during cardiovascular diseases such as hypertension and heart failure (Riegger *et al.* 1985; Packer *et al.* 1987; Packer, 1988; Yemane *et al.* 2010; Littlejohn *et al.* 2013). Neurohumoral activation has a direct impact into morbidity/mortality in these diseases (Cohn *et al.* 1984; Yemane *et al.* 2010). Thus, elucidating the precise cellular mechanisms contributing to altered MNC activity in hypertension is of critical importance.

The amino acid glutamate, acting primarily on ionotropic NMDA receptors (NMDARs) is the major excitatory neurotransmitter within the SON and PVN (van den Pol *et al.* 1990). Binding of glutamate to NMDARs results in an influx of Ca^{2+} that evokes a direct membrane depolarization and the adoption of burst firing activity (Hu & Bourque, 1992; Nissen *et al.* 1995), which optimizes neuropeptide release from the posterior pituitary (Cazalis *et al.* 1985). Importantly, a growing body of evidence supports an elevated glutamate tone (Zhang *et al.* 2017), an increased glutamatergic innervation density (Biancardi *et al.* 2010) and increased expression of NMDARs (Li *et al.* 2014; Glass *et al.* 2015) in the SON and PVN of hypertensive rats.

In addition to evoking membrane depolarization, the NMDAR-mediated Ca^{2+} influx results in an increase in intracellular free Ca^{2+} levels (ΔCa^{2+}) (McBain & Mayer, 1994) affecting in turn a variety of downstream signalling mechanisms, including activation of Ca^{2+} -sensitive channels (Petersen, 2002; Sah & Faber, 2002), changes in the balance of kinase/phosphatase activities (Colbran & Brown, 2004) and stimulation of nitric oxide production (Bredt & Snyder, 1989), all of which could further alter MNC activity.

We recently showed that, in addition to acting on synaptically located NMDARs (sNMDARs) to mediate transient excitatory postsynaptic currents (EPSCs), glutamate also binds to extrasynaptic NMDARs (eNMDARs), activation of which mediates a tonic, sustained excitatory current that strongly stimulates firing activity in MNCs (Fleming *et al.* 2011). Moreover, we showed that eNMDARs (but not sNMDARs) are functionally coupled, in a Ca^{2+} -dependent manner, to the A-type K^+ channel-mediated current I_A (Naskar &

Stern, 2014) and that an augmented eNMDAR– I_A coupling is a critical mechanism contributing to exacerbated MNC activity in renovascular hypertension (RVH) (Zhang *et al.* 2017). However, whether a change in NMDAR– ΔCa^{2+} contributed to the altered NMDAR– I_A coupling and increased MNC activity in RVH rats remains unknown.

The functional consequences of the NMDAR– ΔCa^{2+} are largely dependent on the magnitude and time course of the Ca^{2+} signal, which in turn are determined not only by the amount of Ca^{2+} influx following NMDAR activation, but also by intracellular Ca^{2+} buffering mechanisms, including the endoplasmic reticulum via the sarco/endoplasmic reticulum Ca^{2+} -ATPase (SERCA) pump (Toescu & Verkhratsky, 1998). Surprisingly, the precise spatiotemporal Ca^{2+} dynamics in MNCs following NMDAR activation have not been investigated in detail, and more importantly, whether an altered NMDAR– ΔCa^{2+} dynamic in MNCs occurs during hypertension, contributing in turn to its exacerbated actions, remains unknown. To this end, we performed in this study simultaneous patch-clamp electrophysiological recordings and fast confocal Ca^{2+} imaging to characterize NMDAR– ΔCa^{2+} spatiotemporal dynamics in MNCs in sham and RVH rats.

Methods

Ethical approval

All experimental procedures were in strict compliance with NIH guidelines, and were approved by the Augusta University Institutional Animal Care and Use Committee, and conform to the principles and regulations as described in Grundy (2015).

Animals

Male Wistar rats purchased from Harlan (Indianapolis, IN, USA, 4–5 weeks old) were housed under standardized conditions (12 h:12 h light–dark cycle) with food and water available *ad libitum*. Rats weighing between 150 and 180 g (approximately 5–6 weeks old) were used to induce the renovascular 2K1C Goldblatt hypertension model (RVH), a well-characterized and widely used model. Rats were anaesthetized with isoflurane (3%) throughout the surgery. Following an abdominal incision, the left kidney was exposed, and a 0.2 mm clip was placed over the left renal artery, partially occluding it. Sham rats were subjected to the same surgical procedure, although the

artery was not occluded. Post-operative care included proper management of associated pain (buprenorphine, 0.25 mg kg⁻¹, subcutaneous, as needed). Systolic blood pressure was measured at the beginning of the sixth week post-surgery, using a tail-cuff method. Mean systolic blood pressure values for sham and RVH were 139.9 ± 2.7 (*n* = 14) and 200.0 ± 3.1 mmHg (*n* = 16), respectively (*P* < 0.0001, Student's unpaired *t* test). All rats were used for experiments during the sixth to seventh week post-surgery.

Hypothalamic slices

Rats were anaesthetized with pentobarbital (50 mg kg⁻¹ i.p.), quickly decapitated and brains dissected out. Coronal slices were cut (250 μm thick) utilizing a vibroslicer (Leica VT1200s, Leica Microsystems (Buffalo Grove, IL, USA)) as previously described (Fleming *et al.* 2011). An oxygenated ice cold artificial cerebrospinal fluid (ACSF) was used during slicing (containing in mM): 119 NaCl, 2.5 KCl, 1 MgSO₄, 26 NaHCO₃, 1.25 NaH₂PO₄, 20 D-glucose, 0.4 ascorbic acid, 2.0 CaCl₂ and 2.0 pyruvic acid; pH 7.4; 295–305 mosmol l⁻¹. After sectioning, slices were placed in a holding chamber containing ACSF and kept at room temperature (22°C) until used.

Electrophysiological recordings

Slices were placed in a submersion-style recording chamber, and bathed with solutions (3.0 ml min⁻¹) that were bubbled continuously with a gas mix of 95% O₂–5% CO₂, and maintained at near physiological temperature (32°C). Thin-walled (1.5 mm o.d., 1.17 mm i.d.) borosilicate glass (G150TF-3, Warner Instruments, Sarasota, FL, USA) was used to pull patch pipettes (3–5 MΩ) on a horizontal Flaming/Brown micropipette puller (P-97, Sutter Instruments, Novato, CA, USA). Whole-cell patch-clamp recordings from SON neurons were visually made using differential interference contrast (DIC) videomicroscopy as previously described (Fleming *et al.* 2011). Recordings were obtained with a Multiclamp 700A amplifier (Axon Instruments, Union City, CA, USA). The voltage output was digitized at 16-bit resolution, 10 kHz (Digidata 1440, Axon Instruments), and saved on a computer to be analysed offline using pCLAMP10 software (Axon Instruments). Mean series resistance was 12.5 ± 0.4 MΩ and experiments were discarded in cases in which the series resistance was unstable or changed >20%. The internal solution contained (in mM): 140 potassium gluconate, 0.2 EGTA, 10 HEPES, 10 KCl, 0.9 MgCl₂, 4 MgATP, 0.3 NaGTP and 20 phosphocreatine (Na⁺); pH was adjusted to 7.2–7.3 with 1 mM KOH and the osmolarity was 280–290 mosmol l⁻¹. The ACSF contained (in mM): 85.09 NaCl, 30 TEA, 2.5 KCl, 26 NaHCO₃, 1.25 NaH₂PO₄, 20 D-glucose, 0.4 ascorbic acid,

2.0 CaCl₂ and 2.0 pyruvic acid. Tetrodotoxin (0.5 μM) was added to prevent generation of action potentials. All recordings were obtained in low Mg²⁺ (10 μM MgSO₄) and in the presence of glycine (10 μM) in order to facilitate measurements of NMDA currents (*I*_{NMDA}), as we previously reported (Fleming *et al.* 2011). *I*_{NMDA} was activated by focal, transient application of NMDA via a picospritzer. *I*_{NMDA} current densities were determined by dividing the current amplitude by the cell capacitance, obtained by integrating the area under the transient capacitive phase of a 5 mV depolarizing step pulse, in voltage clamp mode.

Confocal Ca²⁺ imaging

SON neurons were loaded through the patch pipette with fluo-5F pentapotassium salt (100 μM; Thermo Fisher Scientific, Waltham, MA, USA). Once the whole-cell configuration was established, the dye was allowed to dialyse into the cell for at least 15 min before the initiation of the recordings. Calcium imaging was conducted using the Yokogawa real time live cell laser confocal system (CSU-10) combined with a highly sensitive EMCCD camera (iXon+ 885, Andor Technology, South Windsor, CT, USA) (Son *et al.* 2013). Fluorescence images were obtained using a diode-pumped solid-state laser (Melles Griot, Carlsbad, CA, USA), and fluorescence emission was collected at >495 nm. Images were acquired at a rate of 4 frames s⁻¹. The fractional fluorescence (*F*/*F*₀) was determined by dividing the fluorescence intensity (*F*) within a region of interest (ROI; 10 × 10 pixels) by a baseline fluorescence value (*F*₀) determined from 30 images before brief application of NMDA (a period showing no change in intracellular calcium levels), as previously described (Son *et al.* 2013). The ROI was positioned within the cell soma, and care was taken to avoid the cell nucleus. Data were analysed using Andor IQ software (Andor Technology) and Image J (NIH).

Statistical analysis

All values are expressed as means ± SEM. Drug effects in sham and RVH rats were assessed using two-way analysis of variance repeated measures (ANOVA-RM), as indicated. Where the *F* ratio was significant, *post hoc* comparisons were completed using the Bonferroni *post hoc* test. When needed, and as indicated, Student's unpaired *t* test was used to compare basal differences between sham and RVH rats. Pearson's correlation test was used to determine if correlations existed between two parameters. Differences were considered statistically significant at *P* < 0.05 and *n* refers to the number of cells. Statistical significance was tested at the 95% (*P* < 0.05) confidence level. All statistical analyses were conducted using GraphPad Prism (GraphPad Software, San Diego, CA, USA).

Results

NMDA-evoked currents do not differ between sham and RVH rats

To analyse and compare the properties of NMDA currents in MNCs from sham and RVH rats, patched MNCs were held at various membrane potentials and subjected to repetitive focal applications of NMDA (100 μM , 500 ms duration). Mean cell capacitance (sham: 38.5 ± 5.8 pF, RVH: 37.7 ± 1.0 pF) and input resistance (sham: 796.5 ± 58.3 M Ω , RVH: 868.3 ± 32.9 M Ω) did not differ between experimental groups. As shown in the representative examples of Fig. 1A NMDA evoked fast inward currents from holding potentials of -50 mV to 0 mV, reversing to outward currents at positive membrane potentials. Figure 1B shows plots of the mean current amplitude and density, respectively, as a function of the holding potential. Results from a two-way ANOVA indicated an overall small though significantly diminished I_{NMDA} peak amplitude in RVH compared to sham rats ($F = 1.6$, $P < 0.05$, $n = 6$ in each group). However, *post hoc* analysis indicated that no individual differences

were observed for any of the voltages measured. When data were expressed as current density (i.e. normalized by cell capacitance), similar results were observed ($F = 1.6$, $P < 0.05$). Conversely, no differences in I_{NMDA} area were observed between groups ($F = 0.0001$, $P = 0.9$, not shown). As we recently reported, I_{NMDA} reversal potential was not different between MNCs in sham and RVH rats (Zhang *et al.* 2017).

The time course of NMDAR-evoked changes in intracellular somatic Ca^{2+} levels is prolonged in RVH rats

In addition to evoking direct membrane depolarization, activation of NMDARs leads to an increase in intracellular levels of Ca^{2+} . Thus, to compare the NMDAR-evoked changes in intracellular Ca^{2+} (NMDAR- ΔCa^{2+}) between MNCs in sham and RVH rats, we obtained simultaneous patch-clamp and confocal Ca^{2+} imaging recordings in MNCs loaded with fluo-5 (Methods). In order to better detect and assess changes in intracellular Ca^{2+} dynamics, longer puffs of NMDA, but at a lower concentration, were

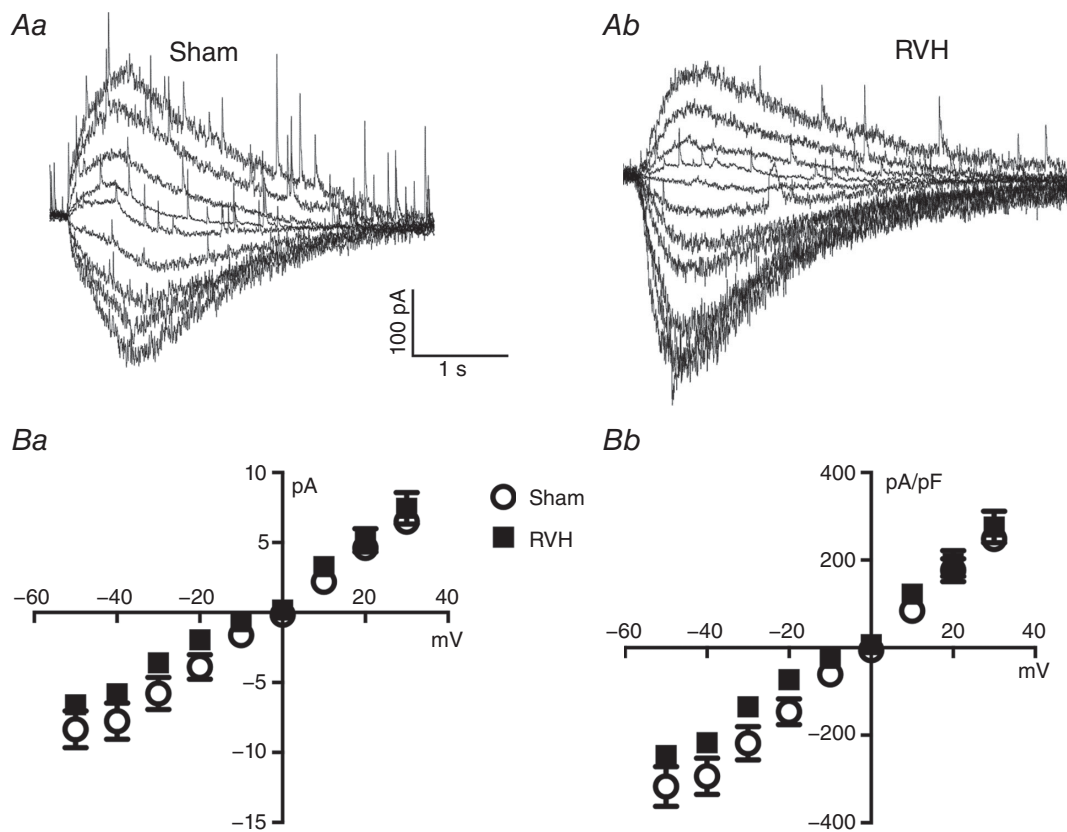


Figure 1. NMDAR activation evokes similar currents in MNCs from sham and RVH rats

A, representative examples of evoked NMDAR-mediated currents (I_{NMDA}) in a MNC from a sham (Aa) and an RVH (Ab) rat, following a puff of NMDA (picrospritzer, 100 μM , 4 p.s.i., 500 ms), while holding the neurons at varying holding potentials (from -50 to $+30$ mV in 10 mV increments). B, mean plots of I_{NMDA} peak amplitude (Ba) and current density (Bb) as a function of the holding V_m in sham and RVH rats ($n = 6$ each).

used ($20 \mu\text{M}$, 5 s). As shown in Fig. 2, focal application of NMDA onto the somata of the recorded neurons evoked a robust increase in somatic $[\text{Ca}^{2+}]_i$ whose time course surpassed the duration of the evoked I_{NMDA} . We found in this set of studies, similar to what we reported in Fig. 1, that the peak amplitude, area and decay kinetics of the focally evoked I_{NMDA} was not different between MNCs in sham and RVH rats ($n = 24$ in each group) (Fig. 3A–C).

Measurements of the NMDAR- ΔCa^{2+} signal revealed no significant differences in the $[\text{Ca}^{2+}]_i$ signal peak amplitude between groups (Fig. 3D). However, the decay time course of the NMDAR- ΔCa^{2+} signal following the NMDA stimulus was notably slower in MNCs from RVH rats. Thus, the decay time constant (τ) in the latter was significantly longer compared to MNCs in sham rats ($P < 0.01$, Fig. 3E). In many cases, as shown in the representative trace in Fig. 2B, $[\text{Ca}^{2+}]_i$ did not return completely to the baseline level before NMDAR stimulation, at least within the time period of the recording. Thus, when this phenomenon was quantified as the percentage NMDAR- ΔCa^{2+} residual at the end of the recording, relative to the $[\text{Ca}^{2+}]_i$ peak, a significantly larger residual $\Delta[\text{Ca}^{2+}]_i$ was observed in MNCs from RVH compared to sham rats ($P < 0.02$, Fig. 3F). The slower decay time course of the NMDAR- ΔCa^{2+} signal in MNCs from RVH rats resulted consequently in a significantly larger NMDAR- ΔCa^{2+} signal area compared to those in sham rats ($P < 0.05$, Fig. 3G). We found no significant

correlations between the magnitude of I_{NMDA} and the magnitude of the evoked $[\text{Ca}^{2+}]_i$ ($R^2 = 0.05$ and 0.18 for sham and RVH, respectively) (Fig. 3H).

In a few instances, we observed a more complex response to the NMDA stimulation, consisting of an initial fast inward component, reflecting the rapid summation of excitatory postsynaptic currents (EPSCs). This response was then followed by a slower, and more persistent I_{NMDA} component. These two phases of the I_{NMDA} response were also clearly reflected in the evoked NMDAR- ΔCa^{2+} signal, in which concomitant fast and slow components were also observed (Fig. 4). These responses were equally observed both in sham and RVH rats ($n = 6/\text{group}$).

Changes in NMDAR-evoked increases in dendritic intracellular Ca^{2+} levels in RVH rats

In a limited number of cases ($n = 5$ and 7 in sham and RVH rats, respectively), intracellular loading with fluo5-F was efficient enough to load and visualize neuronal dendrites, allowing us to monitor also dendritic changes in NMDAR- ΔCa^{2+} signal. A representative image is shown in Fig. 5. For these recordings, we quantified changes at the most distal segment of the visible dendrite. This length ranged from 12.6 to $160.8 \mu\text{m}$. Similar to what we observed for the soma, a significantly prolonged decay time course and a larger NMDAR- ΔCa^{2+} area were observed ($P < 0.02$ for both τ and area) (Fig. 5C). As shown in Fig. 5D,

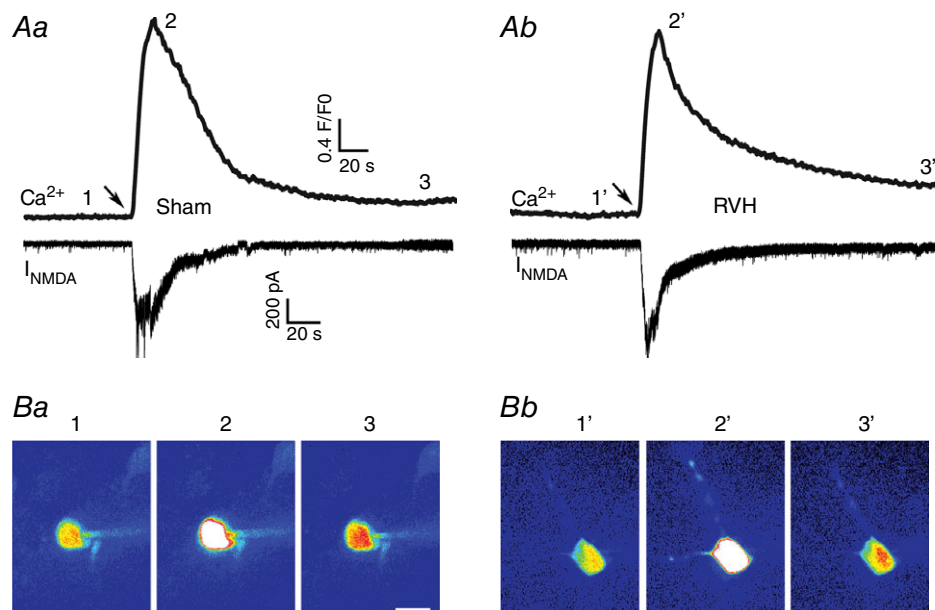


Figure 2. Representative examples of NMDAR-evoked increase in intracellular Ca^{2+} levels in sham and RVH rats

A, simultaneous I_{NMDA} (voltage clamp, lower traces) and intracellular Ca^{2+} (upper traces) measurements in response to a focal brief application of NMDA ($50 \mu\text{M}$, 4 p.s.i., 5 s) in a sham (Aa) and RVH (Ab) rat. B, representative confocal Ca^{2+} images (pseudocolour) of the patched neurons at the time points (1–3/1'–3') indicated in the ΔCa^{2+} traces are shown below. Scale bar in Ba: $15 \mu\text{m}$. Arrows in A point to the time of the NMDA puffs. [Colour figure can be viewed at wileyonlinelibrary.com]

no significant correlations between the dendritic length and ΔCa^{2+} peak ($R^2 = 0.25$ sham and 0.15 RVH), area ($R^2 = 0.50$ sham and 0.01 RVH) or decay τ ($R^2 = 0.001$ sham and 0.13 RVH) were observed ($P > 0.2$ in all cases).

Interestingly, line scans obtained from a subset of dendrites in these recordings indicated that the most predominant dendritic ΔCa^{2+} signals following NMDAR activation occurred within defined dendritic “hot spots”, which likely represent dendritic varicosities (see representative example in Fig. 5B).

A blunted endoplasmic reticulum buffering capacity contributes to the prolonged NMDAR- ΔCa^{2+} in MNCs from RVH rats

A major factor influencing the shape and time course of intracellular Ca^{2+} in MNCs is buffering by the

endoplasmic reticulum (ER) via the sarco/endoplasmic reticulum Ca^{2+} -ATPase (SERCA) pump (Toescu & Verkhratsky, 1998). Thus to determine whether the prolonged NMDAR- ΔCa^{2+} in MNCs from RVH rats was due to a diminished ER Ca^{2+} buffering capacity, we repeated a set of experiments in slices preincubated with thapsigargin (TG) ($3 \mu\text{M}$, 45 min), an endoplasmic reticulum SERCA pump blocker (Lytton *et al.* 1991) that leads to depletion of ER Ca^{2+} stores.

To first test the efficacy of TG in our experimental conditions, MNCs from slices incubated in the presence or absence of TG were exposed to a focal application of caffeine ($50 \mu\text{M}$, 5 s), known to mobilize Ca^{2+} from ER (Komori *et al.* 2010). As shown in Fig. 6, the magnitude of the caffeine-evoked ΔCa^{2+} signal was significantly blunted in slices preincubated in TG ($P < 0.0001$, $n = 7$ and 10 in control and TG, respectively), supporting that

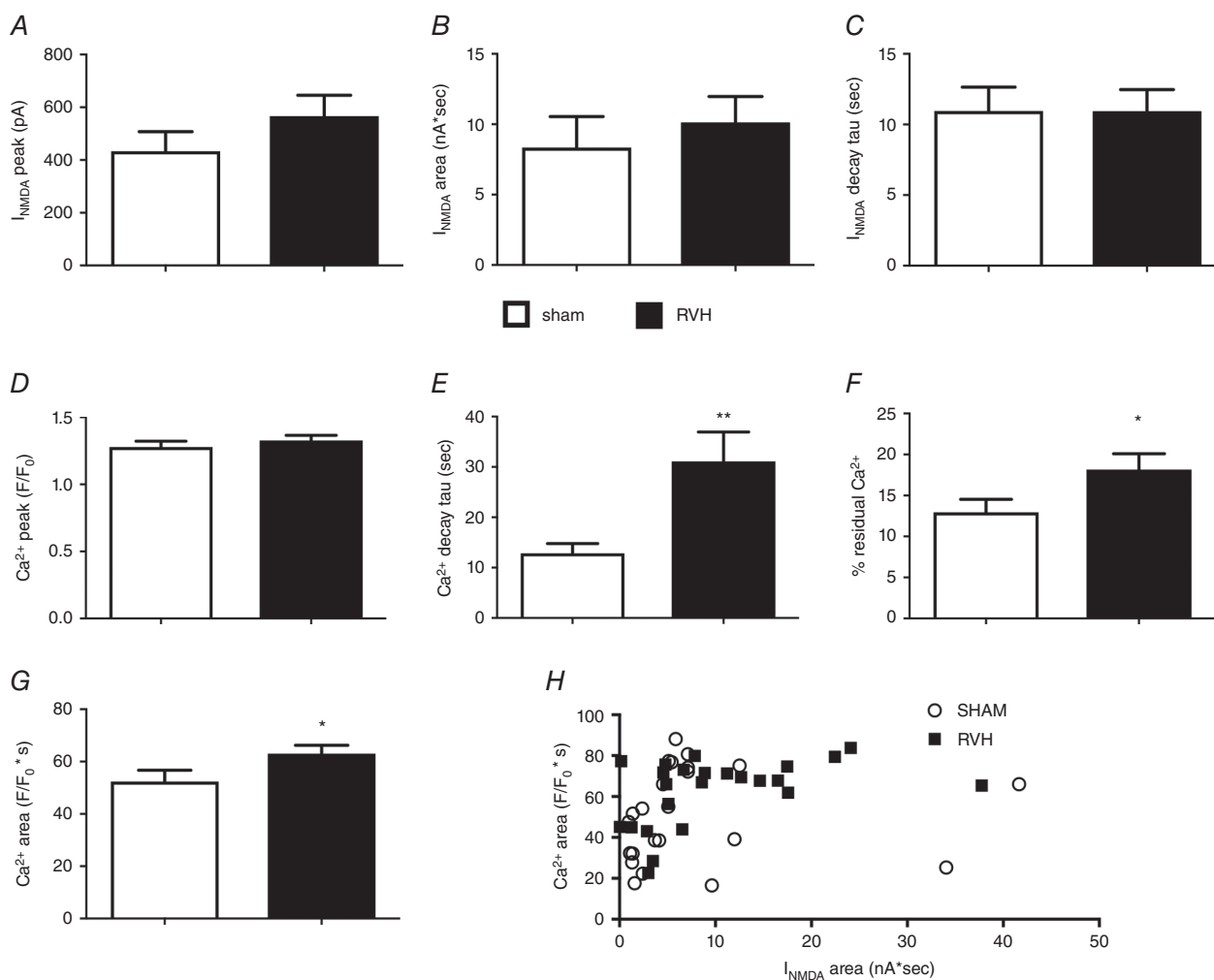


Figure 3. NMDAR-evoked increase in intracellular Ca^{2+} is prolonged in MNCs from RVH rats

Summary of the mean I_{NMDA} peak amplitude (A), area (B) and decay constant (τ) (C) in MNCs from sham and RVH rats. Summary of the mean ΔCa^{2+} peak (D), decay time constant (τ) (E), % residual Ca^{2+} (F) and area (G) in MNCs from sham and RVH rats. H, plot of ΔCa^{2+} area as a function of I_{NMDA} area in MNCs from sham and RVH rats. $n = 24$ in each group. * $P < 0.05$ and ** $P < 0.01$ vs. Sham, unpaired *t* test.

TG significantly blocked SERCA pump activity and ER Ca^{2+} uptake.

In separate sets of studies, we then repeated focal applications of NMDA to MNCs from sham ($n = 19$) and RVH ($n = 26$) rats in slices preincubated in TG as above. Representative examples of these recordings are shown in Fig. 7A and B. Importantly, we found that in slices preincubated in TG, the decay time course of the NMDAR- ΔCa^{2+} in sham rats was slowed down, to the same level as we previously found in RVH rats. Moreover, no further increases in the decay τ were observed in RVH rats in the TG group (Fig. 7Ca). Similar results were observed when the NMDAR- ΔCa^{2+} magnitude (area) was compared among groups (Fig. 7Cb). Thus, the prolonged and enhanced NMDAR- ΔCa^{2+} observed in RVH rats in control conditions was absent in slices preincubated in TG. Unfortunately, we were unable to obtain in this set of studies sufficient MNCs with dendritic labelling, which precluded us from obtaining a similar analysis to that shown in Fig. 5.

Discussion

Using a combination of patch-clamp electrophysiology with simultaneous fast confocal Ca^{2+} imaging in a renovascular hypertensive rat model (RVH), we aimed in this study to determine whether NMDAR-evoked changes in intracellular Ca^{2+} dynamics (NMDAR- ΔCa^{2+}) in MNCs was altered during hypertension, and if so, to identify potential underlying mechanisms. Our main findings indicate that (1) despite a similar magnitude of

NMDA receptor-mediated currents (I_{NMDA}), an altered spatiotemporal profile in the ΔCa^{2+} response was evoked in MNCs of hypertensive rats; (2) the NMDAR- ΔCa^{2+} response was significantly slower and larger over time, resulting in an overall exacerbated ΔCa^{2+} response per unit of I_{NMDA} ; (3) the prolonged and larger NMDA- ΔCa^{2+} responses in MNCs of RVH rats affected both somatic and dendritic compartments; (4) inhibition of the ER SERCA pump activity with thapsigargin prolonged NMDAR- ΔCa^{2+} responses in MNCs of sham rats, but this effect was occluded in RVH rats, equalizing the responses observed in sham and RVH rats in this condition. Taken together, these results support an exacerbated NMDAR- ΔCa^{2+} signalling in MNCs of hypertensive rats, and suggest that a blunted ER Ca^{2+} uptake capacity is a contributing underlying mechanism to this effect.

Exacerbated NMDAR- ΔCa^{2+} signalling in RVH rats: role of altered ER Ca^{2+} buffering capacity

Several studies from our laboratory and others support an exacerbated glutamatergic function in the SON/PVN of hypertensive rats (Li & Pan, 2007; Zheng *et al.* 2011; Gabor & Leenen, 2012; Glass *et al.* 2015). However, the precise underlying mechanisms and pathways ultimately leading to increased neuronal activity and increased neurohumoral outflow from the SON/PVN during this condition remain to be fully elucidated. Here, we focused on addressing the contribution of changes in the spatiotemporal pattern of intracellular Ca^{2+} dynamics, a critical process in determining the overall efficacy and

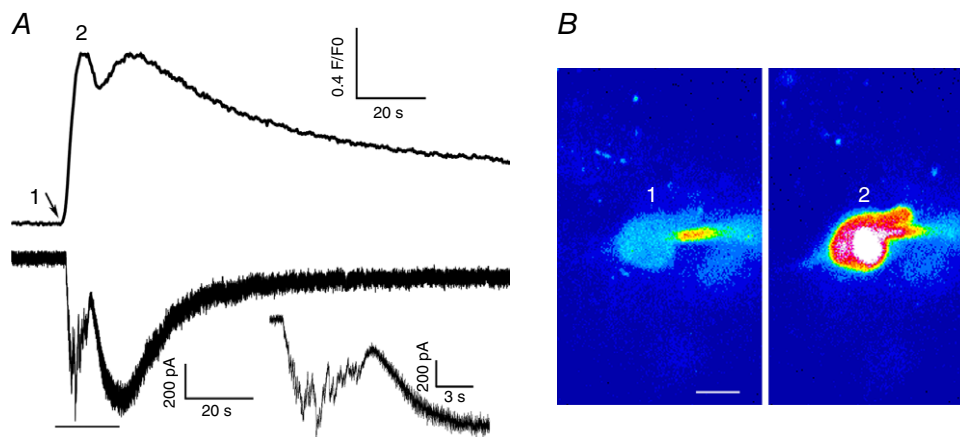


Figure 4. Complex I_{NMDA} and ΔCa^{2+} responses following NMDAR activation in a subset of MNCs

A, representative example of simultaneous I_{NMDA} (voltage clamp, lower trace) and intracellular Ca^{2+} (upper trace) measurements in response to a focal brief application of NMDA, in which an initial fast inward component, likely representing summation of fast EPSPs (arrow, see also expanded inset corresponding to the underlined part of the main trace) is followed by a slower, longer lasting response. These two clearly separate components in I_{NMDA} were also reflected as two separate peaks in the intracellular ΔCa^{2+} response. B, representative confocal Ca^{2+} images (pseudocolour) of the patched neuron at the time points (1 and 2) indicated in the ΔCa^{2+} traces are shown. Scale bar = $10 \mu\text{m}$. The arrow in A points to the time of the NMDA puff. [Colour figure can be viewed at wileyonlinelibrary.com]

downstream actions on membrane excitability that follows the activation of glutamate NMDARs.

One of the key findings in this study is that despite a similar I_{NMDA} magnitude between MNCs from sham and RVH rats, a more prolonged and larger NMDAR- ΔCa^{2+} was observed in the latter. The spatiotemporal pattern

and magnitude of the changes in intracellular Ca^{2+} levels that follow the activation of NMDARs is influenced by a number of different factors, including the expression density of NMDA receptors, the single-channel NMDAR Ca^{2+} permeability, as well as intracellular Ca^{2+} buffering mechanisms. Since Ca^{2+} influx is a major component

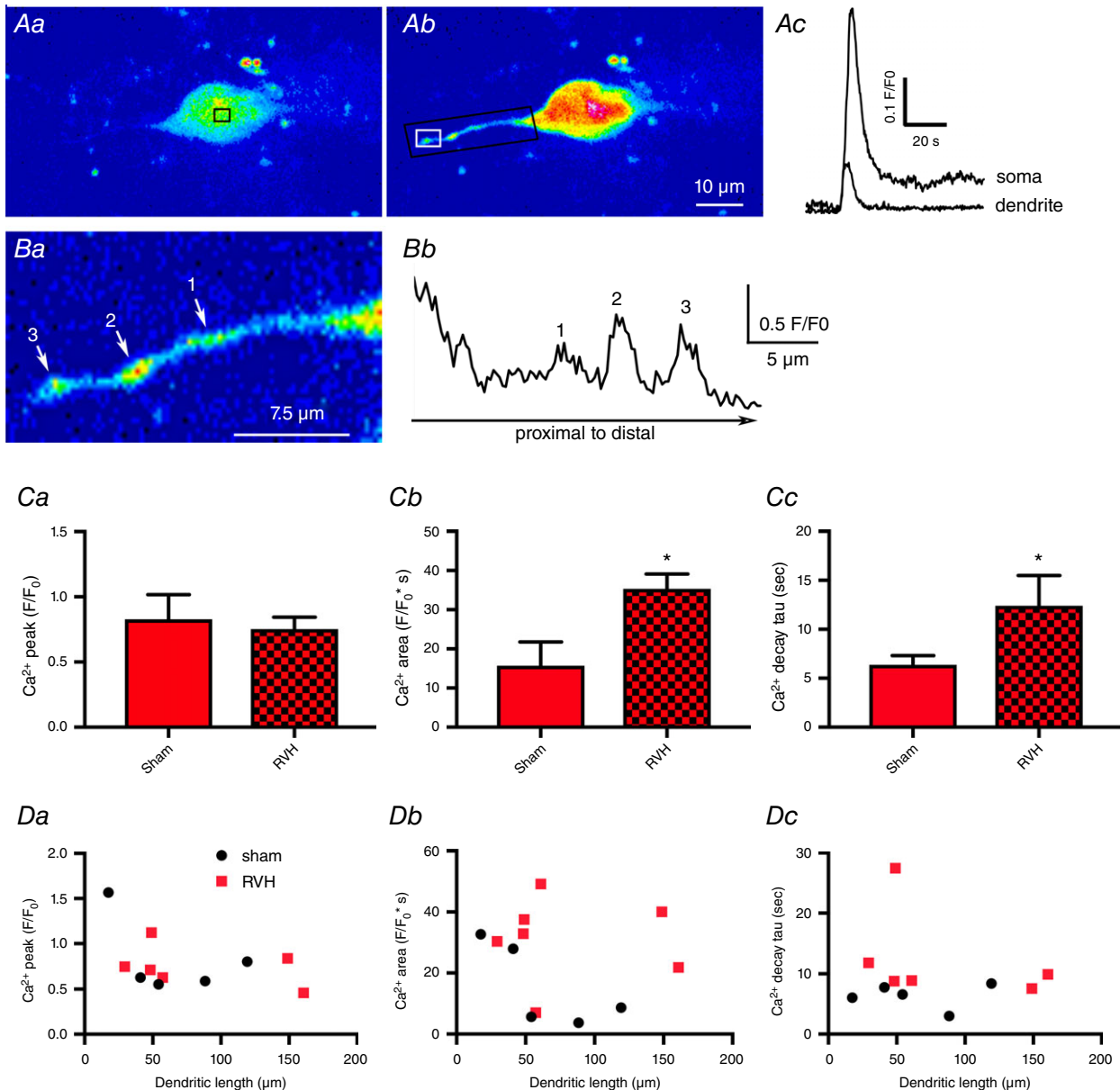


Figure 5. NMDAR-evoked increase in dendritic intracellular Ca^{2+} is prolonged in MNCs from RVH rats

Aa and *Ab*, representative confocal Ca^{2+} images (pseudocolour) of a fluo-5-loaded MNC before (*Aa*) and after (*Ab*) a puff of NMDA ($50 \mu\text{M}$, 4 p.s.i., 5 s). *Ac*, somatic and dendritic ΔCa^{2+} measurements (F/F_0) obtained from the small squared areas indicated in *Aa* and *Ab*, respectively. *Ba*, an expanded dendritic segment (black rectangular area in *Ab*) obtained at the peak of the ΔCa^{2+} response is shown. Note the three dendritic varicosities (1–3), which showed the largest ΔCa^{2+} response, as shown quantitatively in *Bb*, which represents a line scan plot (F/F_0 as a function of distance) along that dendritic segment. *Ca*–*c*, summary of the mean dendritic ΔCa^{2+} peak (*Ca*), area (*Cb*) and decay time constant (τ) (*Cc*) for MNCs in sham ($n = 5$) and RVH ($n = 7$) rats. *Da*–*c*, plots of ΔCa^{2+} peak (*Da*), area (*Db*) and decay time constant (τ) (*Dc*) as a function of the dendritic length from soma. * $P < 0.02$ compared to Sham, unpaired *t* test. [Colour figure can be viewed at wileyonlinelibrary.com]

mediating I_{NMDA} (McBain & Mayer, 1994), and since the magnitude of I_{NMDA} was not different between sham and RVH rats, it is reasonable to argue that an increase in NMDA receptor numbers and/or in Ca^{2+} permeability were not factors contributing to the larger NMDAR- ΔCa^{2+} observed in MNCs from RVH rats.

Following an initial rise in intracellular Ca^{2+} levels, Ca^{2+} buffering and cytosolic clearance mechanisms gradually decrease cytosolic free Ca^{2+} levels, resulting in a slowly decaying Ca^{2+} time course. Thus, a diminished efficacy of Ca^{2+} buffering mechanisms is expected to mostly affect the decay phase of the Ca^{2+} transient. In MNCs, the endoplasmic reticulum Ca^{2+} transport ATPase (ER-SERCA) has been shown to efficiently shape somatic Ca^{2+} transients (Kim *et al.* 2003; Komori *et al.* 2010; Dayanithi *et al.* 2012). Thus, to determine whether a blunted ER-SERCA buffering mechanism contributed to the prolonged NMDA- ΔCa^{2+} in RVH rats, we compared the effects of thapsigargin (TG), a SERCA blocker, on the NMDAR- ΔCa^{2+} signalling both in sham and RVH rats. We found that in MNCs from sham rats, TG significantly prolonged the decay time course and increased the overall magnitude of the NMDAR- ΔCa^{2+} signal to a similar extent to that observed under control conditions in MNCs of RVH rats. Conversely, TG failed to affect the NMDAR- ΔCa^{2+} signal in RVH rats. Taken together, these results are in line with the notion that (1) ER-SERCA efficiently restricts the magnitude and time course of NMDAR- ΔCa^{2+} signalling in MNCs, and (2) that a blunted ER-SERCA buffering capacity contributes to the prolonged NMDAR- ΔCa^{2+} signal observed in MNCs in RVH rats. Other alternative mechanisms, however,

including changes in NMDAR desensitization properties, known to affect I_{NMDA} decay kinetic properties (Jonas & Spruston, 1994) could not be completely ruled out.

It is important to acknowledge that the ER could also act as a source of intracellular free Ca^{2+} levels by releasing stored Ca^{2+} , in most instances, in a Ca^{2+} -dependent manner (i.e. Ca^{2+} -induced Ca^{2+} release) (Hongpaisan *et al.* 2001). In fact, NMDAR activation has been shown to evoke ER- Ca^{2+} release in hippocampal neurons, contributing to the overall NMDAR- ΔCa^{2+} waveform (Emptage *et al.* 1999). In our study, however, TG treatment never resulted in a reduction of the NMDAR- ΔCa^{2+} signal. Taken together, our study indicates that in MNCs, the ER takes up (but does not release) Ca^{2+} in response to NMDAR activation.

The precise mechanism ultimately leading to altered ER Ca^{2+} buffering and enhanced NMDAR- ΔCa^{2+} signalling in RVH rats is at present unknown. ER stress, a process that involves the accumulation of unfolded or misfolded proteins in the ER lumen, has been proposed to be a critical mechanism in the development and maintenance of neurogenic hypertension (Young *et al.* 2012; Chao *et al.* 2013). ER stress could result from various pathological processes, including angiotensin II-mediated oxidative stress (Chao *et al.* 2013), or subsequent to a cytoplasmic Ca^{2+} overload (Richter *et al.* 2016). In fact, sustained NMDAR activation in hippocampal neurons was recently shown to contribute to ER stress via Ca^{2+} overload (Dong *et al.* 2017). Conversely, once established, ER stress affects ER Ca^{2+} homeostasis, furthering in turn cytosolic Ca^{2+} accumulation (Richter *et al.* 2016). Nevertheless, whether the enhanced tonic NMDAR activation that occurs in

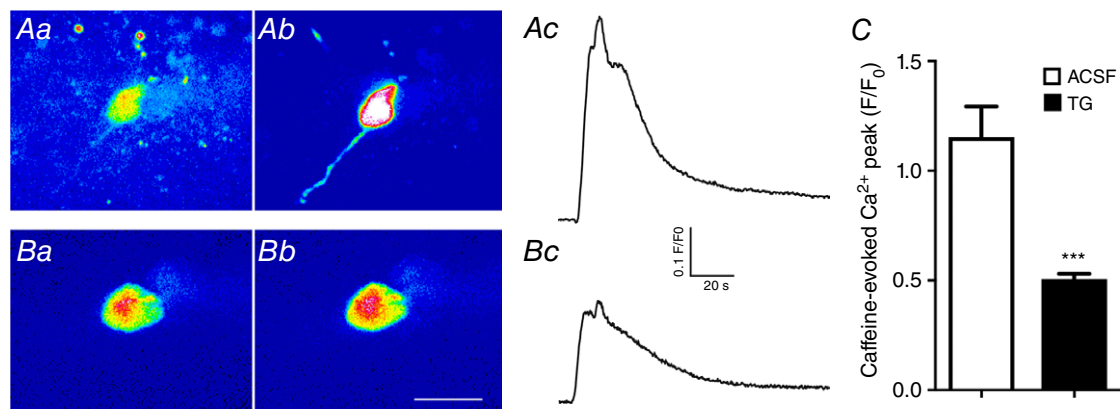


Figure 6. Thapsigargin (TG) blunts caffeine-induced increases in intracellular Ca^{2+} levels

Aa and b, representative confocal Ca^{2+} images (pseudocolour) of a fluo-5-loaded MNC before (Aa) and after (Ab) a puff of caffeine ($50 \mu\text{M}$, 5 s) in control ACSF. Ac, somatic ΔCa^{2+} measurements (F/F_0) in response to caffeine obtained from the same MNC shown in Aa and b. Ba and b, representative confocal Ca^{2+} images (pseudocolour) of a different fluo-5-loaded MNC before (Ba) and after (Bb) a puff of caffeine ($50 \mu\text{M}$, 5 s) in a slice preincubated in TG ($3 \mu\text{M}$, 45 min). Bc, somatic ΔCa^{2+} measurements (F/F_0) in response to caffeine obtained from the same MNC shown in Ba and b. C, summary data of mean ΔCa^{2+} peak amplitude in response to caffeine in slices incubated in normal ACSF ($n = 7$) or in TG ($n = 10$). *** $P < 0.0001$ vs. ACSF unpaired t test. Scale bar in Bb = $20 \mu\text{m}$. [Colour figure can be viewed at wileyonlinelibrary.com]

MNCs during hypertension (Zhang *et al.* 2017) is a critical factor itself contributing to ER stress and disrupted intracellular Ca^{2+} homeostasis in this condition, remains to be determined.

As reported, we observed in some instances a multimodal response to NMDA consisting of an initial fast inward component that reflected the rapid summation of excitatory postsynaptic currents (EPSCs) followed by the most typical slower, and more persistent I_{NMDA} component. While this phenomenon was not further explored in this work, the initial fast component could reflect activation of presynaptic NMDARs resulting in enhanced endogenous neurotransmitter release efficacy, as reported elsewhere (Bouvier *et al.* 2015).

In relation to this, one limitation of our study is that a puff of NMDA, due to the relatively slow and diffuse spatiotemporal profile of agonist delivery, results most likely in the activation of extrasynaptic over synaptic NMDARs, largely because the latter are contained within a spatially restricted structure, and desensitize much more rapidly than eNMDARs, which can remain activated in a sustained manner in the presence of the agonist (Sah *et al.* 1989; Okamoto *et al.* 2009). We recently showed that eNMDARs carry the majority of the charge transfer mediated by glutamate excitatory actions in MNCs, strongly stimulating activity in these neurons (Fleming *et al.* 2011). Moreover, we recently showed that eNMDARs (but not synaptic NMDARs) are functionally

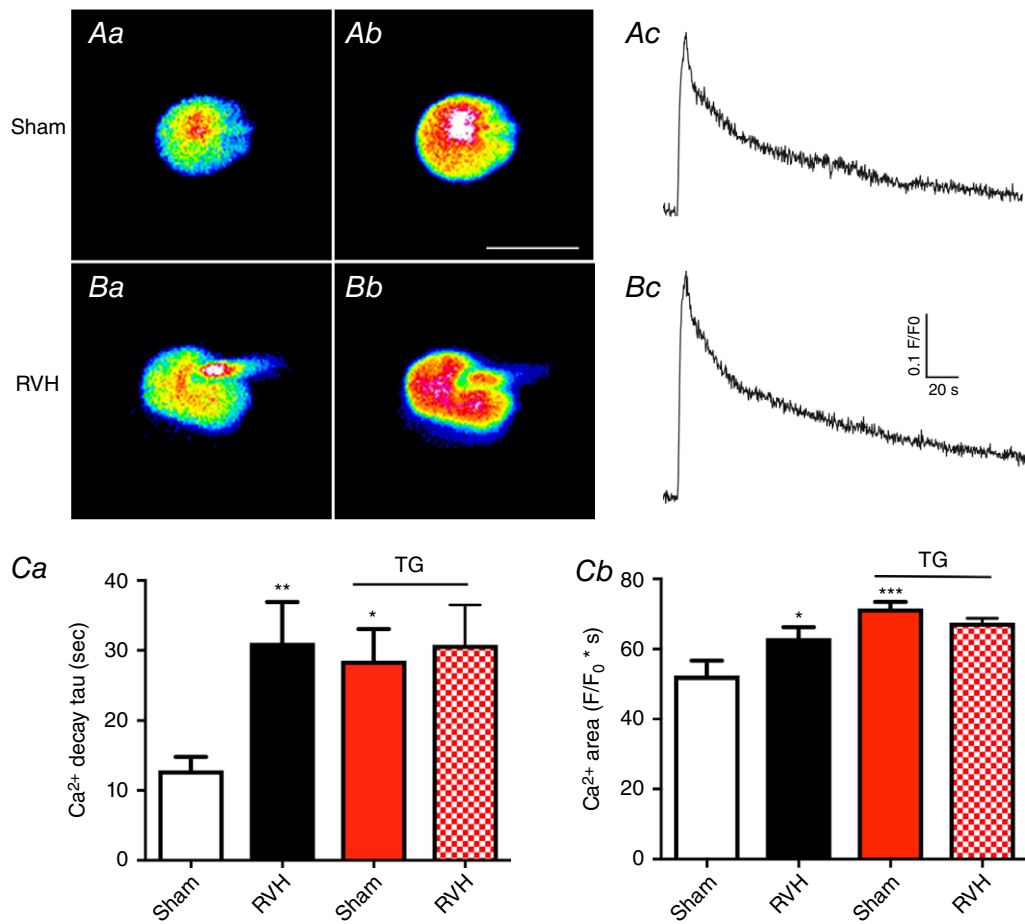


Figure 7. Thapsigargin (TG) blunts caffeine-induced increases in intracellular Ca^{2+} levels

Aa and *b*, representative confocal Ca^{2+} images (pseudocolour) of a fluo-5-loaded MNC in a sham rat before (*Aa*) and after (*Ab*) a puff of NMDA ($50 \mu\text{M}$, 5 s) in slices preincubated in TG. *Ac*, somatic ΔCa^{2+} measurements (F/F_0) in response to NMDA obtained from the same MNC shown in *Aa* and *b*. *Ba* and *b*, representative confocal Ca^{2+} images (pseudocolour) of a fluo-5-loaded MNC in an RVH rat before (*Ba*) and after (*Bb*) a puff of NMDA ($50 \mu\text{M}$, 5 s) in slices preincubated in TG. *Bc*, somatic ΔCa^{2+} measurements (F/F_0) in response to NMDA obtained from the same MNC shown in *Ba* and *b*. *Ca* and *b*, combined summary data of mean ΔCa^{2+} decay time constant (τ) and area, respectively, in MNCs from sham and RVH rats in control ACSF ($n = 24$ and 24 , respectively, for sham and RVH) and in slices preincubated in TG ($n = 19$ and 26 , respectively, for sham and RVH, red columns). Please note that the data for control ACSF is the same as shown in Fig. 3; it was included here for better comparison with data obtained in TG. * $P < 0.05$, ** $P < 0.01$ and *** $P < 0.001$ vs. Sham, Bonferroni's *post hoc* test. Scale bar in *Ab* = $20 \mu\text{m}$. [Colour figure can be viewed at wileyonlinelibrary.com]

coupled, in a Ca^{2+} -dependent manner, to the A-type K^+ channel-mediated current I_A (Naskar & Stern, 2014) and that an augmented eNMDAR– I_A coupling is a critical mechanism contributing to exacerbated MNC activity in RVH rats (Zhang *et al.* 2017). Thus, the fact that we activated eNMDARs in this study is functionally relevant in the context of these previous studies. However, it remains unknown whether glutamate changes in intracellular Ca^{2+} following activation of synaptic NMDARs would be similarly affected in RVH rats.

Another limitation of our study is that we did not distinguish between vasopressin (VP) and oxytocin (OT) MNC phenotypes. Nevertheless, the NMDAR– ΔCa^{2+} signals in sham and RVH rats were relatively consistent across all MNCs tested in each group, suggesting that both cell types were likely affected in hypertensive rats. Future studies will be needed, however, to determine if NMDAR– ΔCa^{2+} signals in VP and OT MNCs are differentially affected in RVH rats.

Functional consequences of altered NMDAR– ΔCa^{2+} signalling in RVH rats

Prolonged and larger NMDAR– ΔCa^{2+} signalling could have numerous downstream consequences on MNC excitability in RVH rats. Critical ion channels and neurotransmitter pathways that influence MNC activity and neurosecretory outflow are modulated in a Ca^{2+} -dependent manner. Thus, a rise in intracellular Ca^{2+} levels following NMDAR activation could lead to activation of inhibitory channels, such as the small conductance Ca^{2+} -dependent K^+ channels (SK), or to excitatory channels such as Ca^{2+} -activated cation (CAN) channels, including TRPM5/6 (Teruyama *et al.* 2011), which would act in a negative or positive feedback, respectively, to the NMDAR-mediated excitatory effect. We recently showed that NMDARs in MNCs are functionally coupled to A-type K^+ channels (Naskar & Stern, 2014), which efficiently affect MNC firing by regulating spike onset and interspike interval during repetitive firing (Bourque, 1988; Luther & Tasker, 2000). Specifically, we showed that NMDAR activation leads to a Ca^{2+} -dependent inhibition of A-type K^+ channels, an effect that potentiates the excitatory effect of NMDAR activation (Naskar & Stern, 2014). Moreover, we also reported that an augmented NMDAR tone contributed to blunted A-type K^+ channel activity, and thus firing discharge in MNCs in RVH rats (Zhang *et al.* 2017). Thus, the results from the present work support the notion that a blunted ER Ca^{2+} buffering capacity could be a contributing mechanism leading to the enhanced NMDAR– I_A coupling and exacerbated firing activity of MNCs during hypertension. Clearly, future studies are warranted to further assess how the various downstream Ca^{2+} -dependent signalling mechanisms are

affected in MNCs during hypertension, as a consequence of the enhanced NMDAR– ΔCa^{2+} signalling in this condition.

We found that the increased NMDAR– ΔCa^{2+} signal observed in MNCs from RVH rats was not only restricted to the soma, but also involved dendritic compartments. In MNCs, this phenomenon is expected to have important physiological consequences. VP and OT are not only released from neurohypophysial terminals into the circulation, but also intranuclearly from the dendrites of MNCs (Ludwig & Leng, 2006). Dendritic release of these neuropeptides is activity- and Ca^{2+} -dependent (Ludwig & Leng, 2006), and activation of NMDARs, via the subsequent increase in intracellular Ca^{2+} , serves as a powerful mechanism to trigger dendritic release (de Kock *et al.* 2004; Son *et al.* 2013). Intranuclear release of VP and OT acts as a powerful autoregulatory mechanism to regulate MNC firing activity and to optimize systemic release (Ludwig & Leng, 1997; Gouzenes *et al.* 1998). Moreover, we recently showed that dendritic release of VP, via diffusion in the extracellular space, stimulates the activity of neighbouring presympathetic neurons, increasing sympathoexcitatory outflow from the PVN (Son *et al.* 2013). Thus, the enhanced NMDAR– ΔCa^{2+} in RVH rats may lead to an augmented dendritic VP release, contributing in turn to enhanced neurohumoral outflow during hypertension.

In summary, results from the present study show that NMDAR– ΔCa^{2+} signalling in MNCs is exacerbated in MNCs from RVH rats, and that a blunted ER Ca^{2+} buffering capacity contributes as an underlying mechanism. Future studies are warranted to further assess the precise mechanisms leading to altered ER function in RVH rats as well as the overall contribution of this mechanism to neurohumoral activation in neurogenic hypertension.

References

- Biancardi VC, Campos RR & Stern JE (2010). Altered balance of gamma-aminobutyric acidergic and glutamatergic afferent inputs in rostral ventrolateral medulla-projecting neurons in the paraventricular nucleus of the hypothalamus of renovascular hypertensive rats. *J Comp Neurol* **518**, 567–585.
- Bourque CW (1988). Transient calcium-dependent potassium current in magnocellular neurosecretory cells of the rat supraoptic nucleus. *J Physiol* **397**, 331–347.
- Bouvier G, Bidoret C, Casado M & Paoletti P (2015). Presynaptic NMDA receptors: Roles and rules. *Neuroscience* **311**, 322–340.
- Bredt DS & Snyder SH (1989). Nitric oxide mediates glutamate-linked enhancement of cGMP levels in the cerebellum. *Proc Natl Acad Sci USA* **86**, 9030–9033.
- Cazalis M, Dayanithi G & Nordmann JJ (1985). The role of patterned burst and interburst interval on the excitation-coupling mechanism in the isolated rat neural lobe. *J Physiol* **369**, 45–60.

- Chao YM, Lai MD & Chan JY (2013). Redox-sensitive endoplasmic reticulum stress and autophagy at rostral ventrolateral medulla contribute to hypertension in spontaneously hypertensive rats. *Hypertension* **61**, 1270–1280.
- Cohn JN, Levine TB, Olivari MT, Garberg V, Lura D, Francis GS, Simon AB & Rector T (1984). Plasma norepinephrine as a guide to prognosis in patients with chronic congestive heart failure. *N Engl J Med* **311**, 819–823.
- Colbran RJ & Brown AM (2004). Calcium/calmodulin-dependent protein kinase II and synaptic plasticity. *Curr Opin Neurobiol* **14**, 318–327.
- Dayanithi G, Forostyak O, Ueta Y, Verkhatsky A & Toescu EC (2012). Segregation of calcium signalling mechanisms in magnocellular neurones and terminals. *Cell Calcium* **51**, 293–299.
- de Kock CP, Burnashev N, Lodder JC, Mansvelter HD & Brussaard AB (2004). NMDA receptors induce somatodendritic secretion in hypothalamic neurones of lactating female rats. *J Physiol* **561**, 53–64.
- Dong Y, Kalueff AV & Song C (2017). *N*-methyl-D-aspartate receptor-mediated calcium overload and endoplasmic reticulum stress are involved in interleukin-1 β -induced neuronal apoptosis in rat hippocampus. *J Neuroimmunol* **307**, 7–13.
- Emptage N, Bliss TV & Fine A (1999). Single synaptic events evoke NMDA receptor-mediated release of calcium from internal stores in hippocampal dendritic spines. *Neuron* **22**, 115–124.
- Fleming TM, Scott V, Joe N, Naskar K, Brown CH & Stern JE (2011). State-dependent changes in astrocyte regulation of extrasynaptic NMDA receptor signalling in neurosecretory neurons. *J Physiol* **589**, 3929–3941.
- Gabor A & Leenen FH (2012). Central neuromodulatory pathways regulating sympathetic activity in hypertension. *J Appl Physiol* (1985) **113**, 1294–1303.
- Glass MJ, Wang G, Coleman CG, Chan J, Ogorodnik E, Van Kempen TA, Milner TA, Butler SD, Young CN, Davisson RL, Iadecola C & Pickel VM (2015). NMDA receptor plasticity in the hypothalamic paraventricular nucleus contributes to the elevated blood pressure produced by angiotensin II. *J Neurosci* **35**, 9558–9567.
- Gouzenes L, Desarmenien MG, Hussy N, Richard P & Moos FC (1998). Vasopressin regularizes the phasic firing pattern of rat hypothalamic magnocellular vasopressin neurons. *J Neurosci* **18**, 1879–1885.
- Grundy D (2015). Principles and standards for reporting animal experiments in *The Journal of Physiology* and *Experimental Physiology*. *J Physiol* **593**, 2547–2549.
- Hongpaisan J, Pivovarova NB, Colegrove SL, Leapman RD, Friel DD & Andrews SB (2001). Multiple modes of calcium-induced calcium release in sympathetic neurons II: a [Ca²⁺]_i- and location-dependent transition from endoplasmic reticulum Ca accumulation to net Ca release. *J Gen Physiol* **118**, 101–112.
- Hu B & Bourque CW (1992). NMDA receptor-mediated rhythmic bursting activity in rat supraoptic nucleus neurones *in vitro*. *J Physiol* **458**, 667–687.
- Jonas P & Spruston N (1994). Mechanisms shaping glutamate-mediated excitatory postsynaptic currents in the CNS. *Curr Opin Neurobiol* **4**, 366–372.
- Kim MH, Lee SH, Park KH & Ho WK (2003). Distribution of K⁺-dependent Na⁺/Ca²⁺ exchangers in the rat supraoptic magnocellular neuron is polarized to axon terminals. *J Neurosci* **23**, 11673–11680.
- Komori Y, Tanaka M, Kuba M, Ishii M, Abe M, Kitamura N, Verkhatsky A, Shibuya I & Dayanithi G (2010). Ca²⁺ homeostasis, Ca²⁺ signalling and somatodendritic vasopressin release in adult rat supraoptic nucleus neurones. *Cell Calcium* **48**, 324–332.
- Li DP & Pan HL (2007). Glutamatergic inputs in the hypothalamic paraventricular nucleus maintain sympathetic vasomotor tone in hypertension. *Hypertension* **49**, 916–925.
- Li DP, Zhu LH, Pachuau J, Lee HA & Pan HL (2014). mGluR5 upregulation increases excitability of hypothalamic presympathetic neurons through NMDA receptor trafficking in spontaneously hypertensive rats. *J Neurosci* **34**, 4309–4317.
- Littlejohn NK, Siel RB Jr, Ketsawatsomkron P, Pelham CJ, Pearson NA, Hilzendeger AM, Buehrer BA, Weidemann BJ, Li H, Davis DR, Thompson AP, Liu X, Cassell MD, Sigmund CD & Grobe JL (2013). Hypertension in mice with transgenic activation of the brain renin-angiotensin system is vasopressin dependent. *Am J Physiol Regul Integr Comp Physiol* **304**, R818–R828.
- Ludwig M & Leng G (1997). Autoinhibition of supraoptic nucleus vasopressin neurons *in vivo*: a combined retrodialysis/electrophysiological study in rats. *Eur J Neurosci* **9**, 2532–2540.
- Ludwig M & Leng G (2006). Dendritic peptide release and peptide-dependent behaviours. *Nat Rev Neurosci* **7**, 126–136.
- Luther JA & Tasker JG (2000). Voltage-gated currents distinguish parvocellular from magnocellular neurones in the rat hypothalamic paraventricular nucleus. *J Physiol* **523**, 193–209.
- Lytton J, Westlin M & Hanley MR (1991). Thapsigargin inhibits the sarcoplasmic or endoplasmic reticulum Ca-ATPase family of calcium pumps. *J Biol Chem* **266**, 17067–17071.
- McBain CJ & Mayer ML (1994). *N*-Methyl-D-aspartic acid receptor structure and function. *Physiol Rev* **74**, 723–760.
- Naskar K & Stern JE (2014). A functional coupling between extrasynaptic NMDA receptors and A-type K⁺ channels under astrocyte control regulates hypothalamic neurosecretory neuronal activity. *J Physiol* **592**, 2813–2827.
- Nissen R, Hu B & Renaud LP (1995). Regulation of spontaneous phasic firing of rat supraoptic vasopressin neurones *in vivo* by glutamate receptors. *J Physiol* **484**, 415–424.
- Okamoto S, Pouladi MA, Talantova M, Yao D, Xia P, Ehrnhoefer DE, Zaidi R, Clemente A, Kaul M, Graham RK, Zhang D, Vincent Chen HS, Tong G, Hayden MR & Lipton SA (2009). Balance between synaptic versus extrasynaptic NMDA receptor activity influences inclusions and neurotoxicity of mutant huntingtin. *Nat Med* **15**, 1407–1413.
- Packer M (1988). Neurohormonal interactions and adaptations in congestive heart failure. *Circulation* **77**, 721–730.

- Packer M, Lee WH, Kessler PD, Gottlieb SS, Bernstein JL & Kukin ML (1987). Role of neurohormonal mechanisms in determining survival in patients with severe chronic heart failure. *Circulation* **75**, IV80–92.
- Petersen OH (2002). Cation channels: homing in on the elusive CAN channels. *Curr Biol* **12**, R520–522.
- Richter M, Vidovic N, Honrath B, Mahavadi P, Dodel R, Dolga AM & Culmsee C (2016). Activation of SK2 channels preserves ER Ca²⁺ homeostasis and protects against ER stress-induced cell death. *Cell Death Differ* **23**, 814–827.
- Riegger GA, Liebau G, Bauer E & Kochsiek K (1985). Vasopressin and renin in high output heart failure of rats: hemodynamic effects of elevated plasma hormone levels. *J Cardiovasc Pharmacol* **7**, 1–5.
- Sah P & Faber ES (2002). Channels underlying neuronal calcium-activated potassium currents. *Prog Neurobiol* **66**, 345–353.
- Sah P, Hestrin S & Nicoll R (1989). Tonic activation of NMDA receptors by ambient glutamate enhances excitability of neurons. *Science* **246**, 815–818.
- Silverman AJ & Zimmerman EA (1983). Magnocellular neurosecretory system. *Annu Rev Neurosci* **6**, 357–380.
- Son SJ, Filosa JA, Potapenko ES, Biancardi VC, Zheng H, Patel KP, Tobin VA, Ludwig M & Stern JE (2013). Dendritic peptide release mediates interpopulation crosstalk between neurosecretory and preautonomic networks. *Neuron* **78**, 1036–1049.
- Teruyama R, Sakuraba M, Kurotaki H & Armstrong WE (2011). Transient receptor potential channel M4 and M5 in magnocellular cells in rat supraoptic and paraventricular nuclei. *J Neuroendocrinol* **23**, 1204–1213.
- Toescu EC & Verkhatsky A (1998). *Principles of Calcium Signalling*. Plenum Press, New York.
- van den Pol A, Wuarin J & Dudek F (1990). Glutamate, the dominant excitatory transmitter in neuroendocrine regulation. *Science* **250**, 1276–1278.
- Yemane H, Busauskas M, Burris SK & Knuepfer MM (2010). Neurohumoral mechanisms in deoxycorticosterone acetate (DOCA)-salt hypertension in rats. *Exp Physiol* **95**, 51–55.
- Young CN, Cao X, Guraju MR, Pierce JP, Morgan DA, Wang G, Iadecola C, Mark AL & Davisson RL (2012). ER stress in the brain subfornical organ mediates angiotensin-dependent hypertension. *J Clin Invest* **122**, 3960–3964.
- Zhang M, Biancardi VC & Stern JE (2017). An increased extrasynaptic NMDA tone inhibits A-type K⁺ current and increases excitability of hypothalamic neurosecretory neurons in hypertensive rats. *J Physiol* **595**, 4647–4661.
- Zheng H, Liu X, Li Y, Sharma NM & Patel KP (2011). Gene transfer of neuronal nitric oxide synthase to the paraventricular nucleus reduces the enhanced glutamatergic tone in rats with chronic heart failure. *Hypertension* **58**, 966–973.

Additional information

Competing interests

None declared.

Author contributions

M.Z. carried out the experiments, analysed, interpreted data and contributed to manuscript writing. J.E.S. advised on the experiments and the analysis, and wrote the manuscript. All authors have approved the final version of the manuscript and agree to be accountable for all aspects of the work. All persons designated as authors qualify for authorship and all those who qualify for authorship are listed.

Funding

This work was supported by an NIH National Heart, Lung, and Blood Institute grant (R01 HL112225) to J.E.S.